

## **Photogalvanic Cells Based on Lyotropic Nanosystems: Toward the use of Liquid Nanotechnology for Personalised Energy Sources**

Jonathan E. Halls,<sup>\*,†</sup> Jay D. Wadhawan<sup>\*</sup>

*Department of Chemistry, The University of Hull,  
Cottingham Road, Kingston-upon-Hull HU6 7RX, United Kingdom*

\*Corresponding authors

<sup>†</sup>Present address: Department of Chemistry, The University of Bath, Claverton Down, Bath BA2 7AY, United Kingdom.

E.mail: [j.e.halls@bath.ac.uk](mailto:j.e.halls@bath.ac.uk) (JEH); [j.wadhawan@hull.ac.uk](mailto:j.wadhawan@hull.ac.uk) (JDW)

### **Electronic Supplementary Information**

#### **Contents**

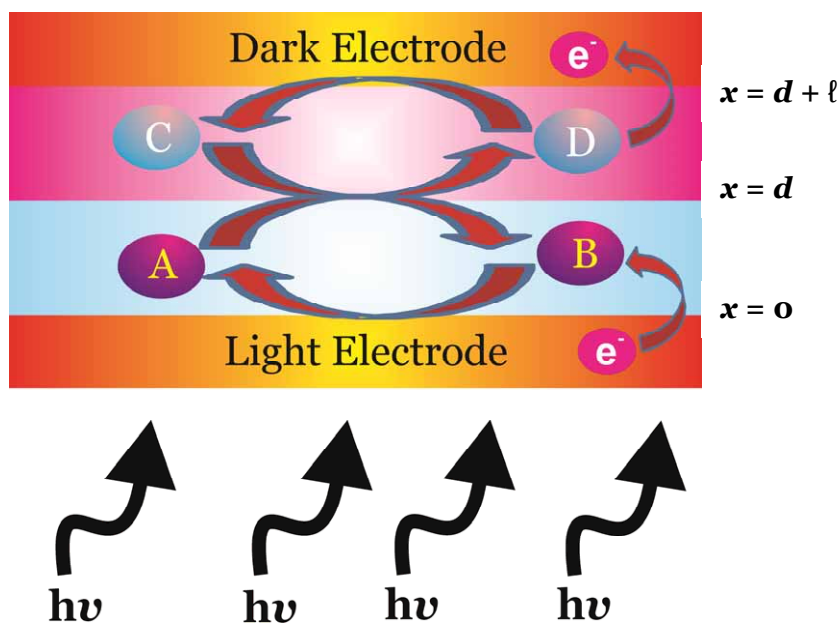
<b>ESI 1: Open Circuit Voltage within Photo-rechargeable Biphasic Batteries</b>	<b>S2</b>
References	S7
<b>ESI 2: Photogalvanic Cells using Aluminium, Nickel or Silver as the Sacrificial Electrode</b>	<b>S9</b>
<b>ESI 3: Electro-less Proton Reduction within Restricted Media</b>	<b>S10</b>
References	S11

### ESI 1: Open Circuit Voltage within Photo-rechargeable Biphasic Batteries

We examine the basic theoretical principles underpinning a *biphasic battery*, with a view to unravel particular insights into the operational viability of such systems, *under conditions of open circuit*.

Consider the biphasic battery system illustrated in Figure S1. It comprises two electrodes parallel to each other, sandwiching a dielectric system comprised of two immiscible liquids (*e.g.* oil and water) that are mutually-saturated. Each of these liquids is loaded with (1) excess supporting electrolyte and (2) a redox-active couple.

**Figure S1:** Schematic illustration of a biphasic battery in which photo-induced electron transfer occurs only at the interface between two immiscible electrolyte systems. The arrows indicate the heterogeneous electron transfer processes in this stacked system.



The liquid | liquid interface is considered to be ideally polarisable, *viz.* there is *no* exchange of ions between the two phases; it is assumed that only one electron is exchanged between the redox pairs across the biphasic interface. In this model, the more dense ( $\alpha$ ) phase contains photoredox-active species A and its redox partner, B ( $B + e^- \rightleftharpoons A$ ). These species are both insoluble within the other liquid phase ( $\beta$ ), which contains the electroactive couple C and D ( $C + e^- \rightleftharpoons D$ ). In the following we assume that *each of the species A, B, C and D have identical concentrations within the liquid electrolytes at zero time*. Thus, at the interface, the equilibrium  $A + C \xrightleftharpoons[k_{off}]{k_{on}} B + D$  is established. Equality of the electrochemical potentials at the interface enables the deduction of the following Nernst equation which describes the variation of the Galvani potential difference ( $\Delta_{\alpha}^{\beta} \phi = \phi^{\beta} - \phi^{\alpha}$ ) with species activity ( $a_i$ ) for these bimolecular heterogenous electron transfer

reactions:  $\Delta_{\alpha}^{\beta}\phi = \Delta_{\alpha}^{\beta}\phi^0 + \frac{RT}{F} \ln \left( \frac{a_B^{\alpha} a_D^{\beta}}{a_A^{\alpha} a_C^{\beta}} \right)$ , where the driving force for the redox reaction through the

interface (the standard interfacial redox potential) is  $\Delta_{\alpha}^{\beta}\phi^0 = E_{A/B}^{0,\alpha} - E_{D/C}^{0,\beta}$ . Note that both of these standard electrode potentials are *referenced to the same scale*. For reversible energy conversion, it is necessary for this reaction to occur unidirectionally under discharge. We, accordingly, consider the case when the formal electrode potentials of the A/B and D/C redox couples are such that  $A + C \rightarrow B + D$  is an endoergic process ( $k_{\text{on}}$  takes a value of zero), and  $B + D \rightarrow A + C$  is spontaneous ( $k_{\text{off}}$  takes a finite, non-zero value), *viz.*  $\Delta E^{0'} = E_{A/B}^{0'} - E_{D/C}^{0'} > 0$ . Thus, *in the dark*, the biphasic battery system will discharge at a rate dependent on the bimolecular electron transfer kinetics, with generation of A and C at the interface. With time, these concentrations will impact on the ratio of B:A and C:D at the surfaces of the two electrodes located in the different phases, causing the cell electromotive force (emf) to diminish. If we are able to charge-up the cell, *viz.* reverse the spontaneous interfacial reaction, then we may increase this open circuit voltage. Indeed, although no power is produced when the cell voltage is at the cell emf, insights into how the latter may be maximised may assist in the engineering of cells with sufficiently large potential differences under conditions of maximum power output.

Let us now consider the case when the cell is *charged* through photochemically-induced electron transfer at the interface. If the interface is illuminated (or if one of the electrodes is transparent or semi-transparent such that the interface may be illuminated), then the photoredox active species contained within the system, species A, may be photo-excited to form an electronically energetic state (A\*). The concentration of this excited state then will vary on the *intensity of the light source, depth of illumination* and the *rate constant* for the exoergic reaction  $A^* + C \rightarrow B + D$ . In noting that the concentrations of the various species are non-uniform, the former may be quantitatively deduced through the following differential equation relating the intensity of the transmitted light (I) to the

individual species concentrations (c),  $\frac{\partial I}{\partial x} = -\epsilon(x)c(x)I$ , where  $\epsilon(x)$  is the extinction coefficient at a

fixed wavelength, and  $x$  is the depth of the illumination probed. This is the case that has been treated by previous workers, albeit under the constraints of analytical approximation and exclusively for homogenous electron transfer.<sup>1,2</sup> In view of the fact that this pathway may not represent the correct chemistry for any developed system, and to simplify our analysis, we assume here that the photo-induced interfacial electron transfer is:  $A + C \rightarrow B + D$ , *viz.* the electron transfer is treated as an *optical charge transfer process*. Such processes are well-established within the literature,<sup>3</sup> such as the electron transfer reaction occurring between *N*-methylphenothiazine and tetrachlorobenzoquinone within an intimate complex of the two species.<sup>3b</sup> This assumption still allows for this photo-induced electron transfer process to be described through the framework of the Marcus theory (*vide infra*).<sup>3</sup>

Thus, assuming that diffusion-only mass transport applies (the cell thickness is *geometrically restricted*, and both phases are assumed to be fully electrochemically-supported), the biphasic battery emf may be deduced through the solution of Fick's second law for each species (where we additionally assume that the cell is adequately described using one spatial dimension):

$$\frac{\partial c_A}{\partial t} = D_A \frac{\partial^2 c_A}{\partial x^2}; \quad \frac{\partial c_B}{\partial t} = D_B \frac{\partial^2 c_B}{\partial x^2}; \quad \frac{\partial c_C}{\partial t} = D_C \frac{\partial^2 c_C}{\partial x^2}; \quad \frac{\partial c_D}{\partial t} = D_D \frac{\partial^2 c_D}{\partial x^2}$$

subject to the following pertinent boundary conditions, where all symbols retain their usual meanings. Note that, for completeness, the electrode kinetics are given through a Butler-Volmer formalism, with transfer coefficient of  $1/2$ ; a future work will examine the solution for the case of a non-zero current flowing within the cell.<sup>4</sup>

$$\begin{aligned} t \leq 0 \quad 0 \leq x < d \quad c_A = A_0; c_B = B_0; c_C = c_D = 0 \\ x = d \quad c_A = A_0; c_B = B_0; c_C = C_0; c_D = D_0 \\ d < x \leq (d + \ell) \quad c_A = c_B = 0; c_C = C_0; c_D = D_0 \end{aligned}$$

$$\begin{aligned} t > 0 \quad x = 0 \quad -D_B \left( \frac{\partial c_B}{\partial x} \right)_{x=0} = D_A \left( \frac{\partial c_A}{\partial x} \right)_{x=0} = -\frac{i_L}{FS} = -k_s e^{-(1/2)\xi \{ (c_B)_{x=0} - (c_A)_{x=0} e^{\xi} \}} \\ x = d + \ell \quad D_D \left( \frac{\partial c_D}{\partial x} \right)_{x=d+\ell} = -D_C \left( \frac{\partial c_C}{\partial x} \right)_{x=d+\ell} = -\frac{i_D}{FS} = -k_{s_2} e^{-(1/2)\xi_2 \{ (c_C)_{x=d+\ell} - (c_D)_{x=d+\ell} e^{\xi_2} \}} \end{aligned}$$

$$\text{where } i_L = -i_D = 0 \text{ and } \xi = \frac{F}{RT} (E_L - E_{A/B}^0); \xi_2 = \frac{F}{RT} (E_D - E_{D/C}^0), \text{ so that } \xi_{oc} = \xi - \xi_2$$

$$x = d \quad D_A \left( \frac{\partial c_A}{\partial x} \right)_{x=d} = D_C \left( \frac{\partial c_C}{\partial x} \right)_{x=d} = k_{on} c_A c_C - k_{off} c_B c_D$$

For open circuit conditions, the ratio of the redox partners at each electrode allows the determination of the individual electrode potentials through a Nernst formulation, *viz.*  $\frac{c_B}{c_A} = e^{\xi}$ ;  $\frac{c_C}{c_D} = e^{\xi_2}$ . In order

to obtain a degree of generality for the solution of the transport equations, the above were recast into adimensional variables for: time,  $\theta = \frac{t}{\tau}$ , where  $\tau$  is the length of the experimental observation;

space,  $y = \frac{x}{\sqrt{D_A \tau}}$ , and with concentrations normalised with respect to the sum of the initial

conditions of species A and B, *viz.*  $(A_0 + B_0)$ . We additionally assume that the diffusion coefficients of species B and A are identical; *mutatis mutandis* for species D and C. The effect of this is to simplify the problem to merely calculating the concentrations pertaining to species A and C. Thus, numerical simulation in these reduced variables was undertaken using the Backward Implicit finite difference

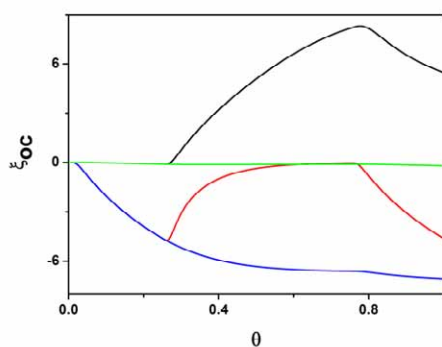
method, with a grid split such that  $d = \ell = \frac{1}{2} \sqrt{D_A \tau}$  (half of the diffusion length developed through

reaction at the liquid | liquid interface in each phase, based on an Einstein-Smoluchowski view, and under the assumption of very dilute solutions – the value of all initial concentrations was set to 1.0 mM), with explicit application of the boundary condition at  $x = d$  at  $t = 0$  to initiate the depletion

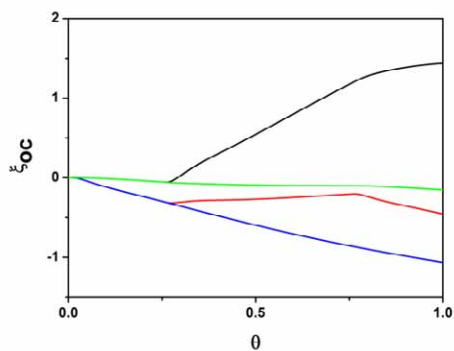
and formation of species. In this way, the simulation was able to be run over both phases through a back-to-back grid approach, with each phase being treated separately, except at the interface. Convergent results were obtained using  $2 \times 10^4$  spatial nodes with  $10^5$  temporal steps in simulations requiring approximately three minutes of computing time.

**Figure S2:** Variation in the cell emf with time in the presence ( $0.25 \leq \theta \leq 0.75$ ) and absence ( $\theta < 0.25$  and  $\theta > 0.75$ ) of light to drive the electron transfer between species A and C. Initial concentrations of all species was set at 1.0 mM, with the real time set at 1000 s. (a),  $D_A = D_C = 10^{-5} \text{ cm}^2 \text{ s}^{-1}$ ;  $D_A = D_C = 10^{-5} \text{ cm}^2 \text{ s}^{-1}$ ; (b)  $D_A = 10D_C = 10^{-5} \text{ cm}^2 \text{ s}^{-1}$ ; (c)  $10D_A = D_C = 10^{-5} \text{ cm}^2 \text{ s}^{-1}$ . Key: black:  $k_{on} = 10^4 k_{off} = 10^{-3} \text{ m}^4 \text{ mol}^{-1} \text{ s}^{-1}$ ; red:  $k_{on} = k_{off} = 10^{-3} \text{ m}^4 \text{ mol}^{-1} \text{ s}^{-1}$ ; blue:  $k_{on} = 10^{-4} k_{off} = 10^{-7} \text{ m}^4 \text{ mol}^{-1} \text{ s}^{-1}$ ; green:  $k_{on} = k_{off} = 10^{-7} \text{ m}^4 \text{ mol}^{-1} \text{ s}^{-1}$ .

(a)



(b)



(c)

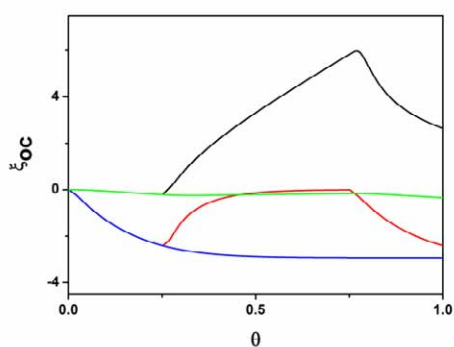


Figure S2 illustrates the results of the simulations, run with open circuit discharge ( $k_{on} = 0$ ) for the first and last 25% of the dimensionless time, with the middle 50% being for the case when  $k_{on}$  takes a non-zero value. Various workers,<sup>5</sup> have explored electron transfer kinetics at both polarised and non-polarised liquid | liquid interfaces. In all cases they observe a Marcus-type variation of the electron transfer rate constant with driving force, with a maximum value for the bimolecular rate constant being reported<sup>18</sup> as  $\sim 10^2 \text{ cm M}^{-1} \text{ s}^{-1} = 10^{-3} \text{ m}^4 \text{ mol}^{-1} \text{ s}^{-1}$ . Taking this value, then, as the maximum value for either  $k_{on}$  or  $k_{off}$ , and considering only pragmatic limiting scenarios, we note from Figure S2a that, when the transport rate for all species is identical, maximum photovoltages occur when the ratio of the two bimolecular rate constants,  $\frac{k_{on}}{k_{off}}$ , is greatest (*viz.* fast charge, slow discharge), as expected;

maximising the ratio  $\frac{k_{off}}{k_{on}}$  is *not* useful – the cell stays in discharge mode – it is not able to be charged

sufficiently rapidly with light energy, irrespective of the light intensity. In this case,  $\xi_{oc}$  is always negative, a situation which we will ascribe to being in *dimensionless reverse polarity mode*. This is not necessarily the same as *true* reverse polarity of the cell, since  $\xi_{oc} = \frac{F}{RT}(E_L - E_D) - \frac{F}{RT}\Delta E^0$ .

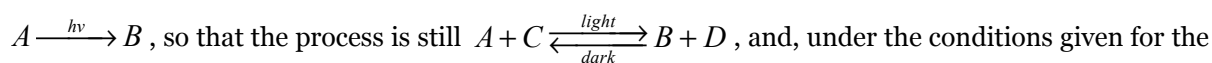
Interestingly, if the system is fast in both charge and discharge, the cell rapidly moves in to dimensionless reverse polarity under open circuit discharge, with the cell emf reaching a quasi-photo-stationary-state upon illumination, with both electrodes taking, more or less, the same dimensionless potential. This scenario translates as the case when the measured cell voltage *equals* the difference between the formal redox potentials of the involved redox couples. Conversely, slow charge and discharge kinetics result in the cell essentially retaining its initial potential – there is little perturbation of the concentrations of the species under open circuit conditions, so that the maximum voltage that can be produced by this cell in real terms is  $\Delta E^0$ .

It thus follows that, for the cell to operate successfully in both discharge and charge modes either  $k_{on}$  needs to be very much bigger than  $k_{off}$ , or, if these rate constants are similar in size,  $\Delta E^0$  needs to be as large and positive as possible; the discharge kinetics should ideally fall within the Marcus inverted region. These conclusions are valid for the case when diffusion rates in both phases are identical. What happens if this is not the case? Intuitively, we expect the observation of *smaller* cell voltages – the rate of communication of the occurrence of the interfacial reaction to the electrodes is reduced. This is indeed observed, as indicated in Figure S2, panels b and c, where it is clear that the trends observed for the four limiting cases are similar to those of the identical diffusion regime, and it becomes apparent that, as expected, although the system discharges more slowly, it also requires *longer* to charge to constant capacity. Note that although the simulated cases in Figures S2b and S2c are still for  $d$  and  $\ell$  being of identical sizes, except that this defined by  $\frac{1}{2}\sqrt{D_A\tau}$ , so that the size of the simulation space, in real terms, is recognised to be *smaller* in Figure S2c compared with Figures

S2a and S2b. This is why, in spite of the similarity of trends, the value of the dimensionless cell emfs are *smaller* for Figure S2b ( $D_A = 10^{-5} \text{ cm}^2 \text{ s}^{-1}$ ,  $D_C = 10^{-6} \text{ cm}^2 \text{ s}^{-1}$ ) compared with Figure S 2c ( $D_A = 10^{-6} \text{ cm}^2 \text{ s}^{-1}$ ,  $D_C = 10^{-5} \text{ cm}^2 \text{ s}^{-1}$ ).

In summary, then, the simulations illustrate that the maximum value of the open circuit voltage occurs when (1)  $\Delta E^0$  is biggest, and (2) when  $\xi_{oc}$  is largest. Whilst these conditions may seem intuitive, in considering (2), it is important to recognise the rôle played by the kinetics of the electron transfer event at the liquid | liquid interface: in general this follows a Marcus-type relationship, in that as the driving force for electron transfer increases, the rate constant increases to a maximum, and then *decreases* with further increase in  $-\Delta G^0$  - the so-called inverted region. *It thus follows that for maximum cell emf under illumination (and noting that this may impact on the maximum power produced), the redox couples in the phases  $\alpha$  and  $\beta$  should be selected such that they exist within the Marcus-inverted region, since then the spontaneous discharge process takes place as pathologically slowly as possible.*

However, there is an additional potential mechanism for a biphasic battery to operate which we now address: what if there is no interfacial Faradaic reaction, but, rather, there is a photo-induced redox reaction in one phase, causing a photovoltage to be developed at the electrode located therein, with the potential of the other electrode controlled by a non-photo-active redox couple within the other phase? An example of this situation is the case when the photo-induced electron transfer is reaction with the solvent comprising the pertinent phase. Then the process is kinetically pseudo-first order:



previous system, the transport equation for species A now becomes  $\frac{\partial c_A}{\partial t} = D_A \frac{\partial^2 c_A}{\partial x^2} - k_f c_A + k_b c_B,$

with the boundary conditions identical, except at  $x = d$ , which is now replaced by a Neumann (no-flux)

condition:  $D_A \left( \frac{\partial c_A}{\partial x} \right)_{x=d} = D_C \left( \frac{\partial c_C}{\partial x} \right)_{x=d} = 0.$  In the above,  $k_f$  is maximally ten times the

Smoluchowski diffusion-limited bimolecular rate constant, and so takes a maximum value of  $\sim 10^{11} \text{ s}^{-1}$ . However,  $k_b$  refers to the back-reaction between the reduced form of the solvent and the oxidised form of species A. Strictly, this is not a pseudo-first-order reaction. Nevertheless, if species B is stable, and the counter ion is unstable (because reduction has occurred dissociatively, either in concert with the electron transfer, or due to fast stepwise kinetics<sup>6</sup>), we recognise that this system can then be made to store light energy –  $k_b$  takes the limiting value of zero, and the system behaves as a photo-battery. The full theoretical analysis of this type of cell will be given in a future work.<sup>4</sup>

## References

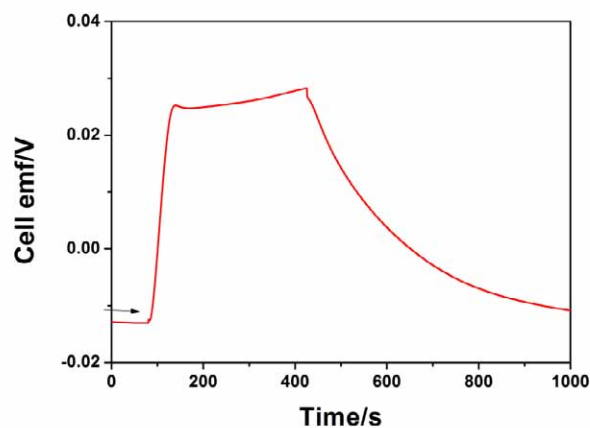
1. (a) M. D. Archer, *J. Appl. Electrochem.*, 1975, 5, 17; (b) C.-T. Lin, N. Sutin, *J. Phys. Chem.*, 1976, 80, 97; (c) W. J. Albery, M. D. Archer, *Electrochim. Acta*, 1976, 21, 1155; (d) W. J. Albery, M. D. Archer, *J. Electrochem. Soc.*, 1977, 124, 688; (e) W. J. Albery, M. D. Archer, *Nature*, 1977, 270, 399; (f) W. J. Albery, M. D. Archer, *J. Electroanal. Chem.*, 1978, 86, 1; (g) W. J. Albery, M. D. Archer, *J. Electroanal. Chem.*, 1978, 86, 19; (h) W. J. Albery, A. W. Foulds, *J. Photochem.*, 1979, 10, 41; (i) M.

- D. Archer, M. I. C. Ferreira, in J. Connolly (ed.), *Photochemical Conversion and Storage of Solar Energy*, 1980, Academic Press, San Diego, p.201; (j) W. J. Albery, *Acc. Chem. Res.*, 1982, **15**, 142; (k) M. D. Archer, *Specialist Periodical Reports on Photochemistry*, 1995, volume 6, The Chemical Society, London, p.739.
- (a) R. Gomer, *Electrochim. Acta*, 1975, **20**, 13; (b) W. D. K. Clark, J. A. Eckert, *Solar Energy*, 1975, **17**, 147; (c) D. E. Hall, J. A. Eckert, N. N. Lichtin, P. D. Wildes, *J. Electrochem. Soc.*, 1976, **123**, 1705; (d) P. D. Wildes, N. N. Lichtin, *J. Am. Chem. Soc.*, 1978, **100**, 6568; (e) J. C. M. Brokken-Zijp, M. S. de Groot, *Chem. Phys. Letts.*, 1980, **76**, 1; (f) J. C. M. Brokken-Zijp, M. S. de Groot, P. A. J. M. Hendriks, *Chem. Phys. Letts.*, 1981, **81**, 129.
  - T. J. Meyer, *Prog. Inorg. Chem.*, 1983, **30**, 389; (b) R. Foster, *Organic Charge-Transfer Complexes*, Academic Press, New York, 1973.
  - J. E. Halls, J. D. Wadhawan, manuscript in preparation.
  - (a) M. Tsionsky, A. J. Bard, M. V. Mirkin, *J. Phys. Chem.*, 1996, **100**, 17881; (b) M. Tsionsky, A. J. Bard, M. V. Mirkin, *J. Am. Chem. Soc.*, 1997, **119**, 10785; (c) A. L. Barker, P. R. Unwin, S. Amemiya, J. Zhou, A. J. Bard, *J. Phys. Chem. B*, 1999, **103**, 7260; (d) F. Li, A. L. Whitworth, P. R. Unwin, *J. Electroanal. Chem.*, 2007, **602**, 70; (e) Z. Ding, D. J. Fermin, P.-F. Brevet, H. H. Girault, *J. Electroanal. Chem.*, 1998, **458**, 139; (f) N. Eugster, D. J. Fermin, H. H. Girault, *J. Phys. Chem. B*, 2002, **106**, 3428; (g) P. Sun, F. Li, Y. Chen, M. Zhang, Z. Zhang, Z. Gao, Y. Shao, *J. Am. Chem. Soc.*, 2003, **125**, 9600.
  - See, for example, J.-M. Savéant, *Elements of Molecular and Biomolecular Electrochemistry*, 2006, Wiley, New York.

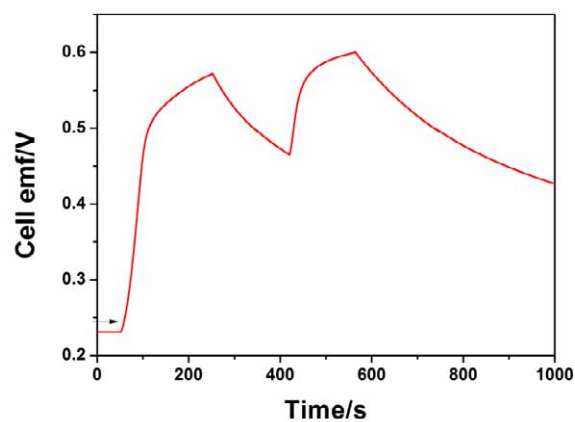
## ESI 2: Photogalvanic Cells using Aluminium, Nickel or Silver as the Sacrificial Electrode

**Figure S3:** Variation of the open circuit voltage of several types of galvanic cells based on the  $L_{\alpha}$  phase of Brij 30 in the presence of chopped light at 350 nm (bandwidth 30 nm), of intensity  $1.8 \text{ mW cm}^{-2}$ . The phase was doped with (a) 0.5 mmol PMe, 0.1 mmol  $\text{AgNO}_3$ ; (b) 0.6 mmol PMe, 0.15 mmol  $\text{NiSO}_4$ ; (c) 0.5 mmol PMe, 3.0 mmol  $\text{AlCl}_3$ . The liquid crystals in panel (e) had the aqueous subphase doped with potassium chloride; those in panels (b), and (c) had oxygen rigorously removed from the devices. The devices were constructed using an ITO illuminated electrode, and a dark electrode constructed from (a) Ag, (b) Ni and (c) Al. The electrode separation was (a) 0.25 mm, (b) 0.5 mm and (c) 1.0 mm. The arrow indicates the variation of the dark cell emf immediately prior to illumination.

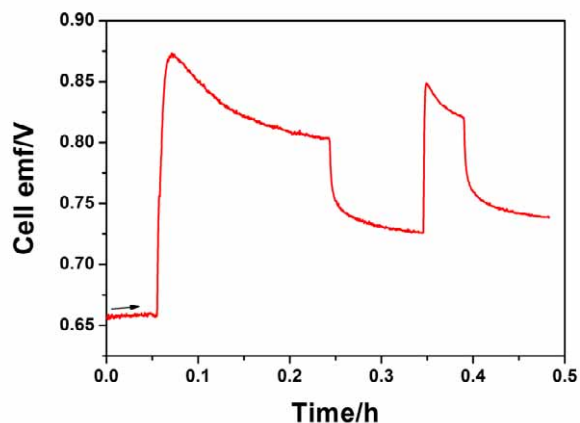
(a)



(b)



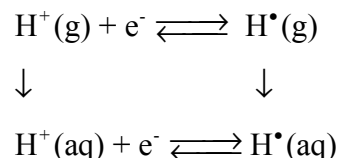
(c)



### ESI 3: Electro-less Proton Reduction within Restricted Media

Proton reduction to form dihydrogen in bulk aqueous solution is energetically unfavoured by the large ionisation energy of hydrogen atoms *and* the large hydration energy of protons, as evidenced by considering the following energy cycle (*q.v.* Scheme S1 and Table S1).

**Scheme S1:** Thermodynamic cycle for proton reduction to hydrogen atoms.



Note that we let the electrons keep their rest energy in vacuum; we shall not consider additional work terms.<sup>S1</sup>

Dihydrogen formation is, however, thermodynamically favoured as a result of the union between two hydrogen atoms, which liberates  $-203.30 \text{ kJ mol}^{-1}$  under standard conditions,<sup>S2</sup> so that the proton/hydrogen atom redox couple tantamounts to behaving as a potential energy barrier to the proton/dihydrogen process. For electrochemical reduction of protons, the adsorption of hydrogen atoms onto the electrode surface essentially acts as a conduit to lowering this potential energy barrier.

The *electro-less* reduction of protons in aqueous solution can then realistically only be achieved under *mild* conditions if there exists a strategy for the partial desolvation of the proton, so that its hydrated cluster is *smaller* than thirteen water molecules.<sup>S3</sup> This may be possible using the restricted media afforded by the micellar palisade layer within lyotropic liquid crystals.<sup>S4</sup> What size then should the hydrated proton be, for this to be possible? Considering the data in Table S1, it appears that *if the size of the hydrated proton is approximately half of that when it exists in bulk water*, the energy required to produce hydrogen atoms through proton reduction is essentially identical to that required to reduce protons electrochemically to form gaseous dihydrogen in bulk aqueous solution at pH 0 ( $-4.44 \text{ eV}$ ).<sup>S2</sup> In noting that the hydration energy of hydrogen atoms has been suggested to be essentially identical to that of dihydrogen,<sup>S5</sup> it follows that dihydrogen evolution is likely thermodynamically viable within such restricted aqueous media (assuming the hydration free energy for hydrogen atoms does not vary significantly as the water clusters become smaller). However, importantly,  $\text{H}_2$  can only form through  $\text{H}^\bullet$  dimerisation under these conditions; if the concentration of the latter is too low,  $\text{H}_2$  will not form readily, thereby leading to the notion of  $\text{H}_2$  evolution modulated by proton *availability*.

Thus, considering the liquid nanostructures employed in this work, we see that the  $\text{L}_\alpha$  phase (with an estimated micellar palisade layer of *ca.*  $9.2 \text{ \AA}$ , with estimated headgroup surface area of <sup>S6</sup>  $36.4 \text{ \AA}^2$ ), should accommodate protons within the palisade layer structure in a non-bulk state – we estimate at most nine water molecules within the proton solvation shell. This should encourage proton reduction to hydrogen atoms, although we note that thermodynamics will be offset by proton co-ordination to

the ethylene oxide moieties. Thus, *any strategy to decrease the inter-surfactant spacing would aid in keeping the protons in a partially-desolvated state, and would facilitate H<sub>2</sub> formation provided the proton concentration is sufficiently high.*

Taking this further, in noting that the natural hydrogenases are thought to incorporate H<sub>2</sub> channels which are at least as big as xenon,<sup>S7</sup> with H<sup>+</sup> reduction mediated by the active site under the external electrochemical control,<sup>S8</sup> it is tempting to speculate that proton reduction may be facilitated by those ions existing in a partially-desolvated state.

**Table S1:** Thermodynamic data required to estimate the absolute potential for proton reduction to hydrogen for the proton in various solvation states.<sup>a</sup>

Species	<sup>b</sup> $\Delta G_{\text{hydration}}^{\text{(H+(g)}\rightarrow\text{H+(aq))}}$ /kJ mol <sup>-1</sup>	<sup>c</sup> $\Delta G_{\text{ionisation}}^{\text{(H(g)}\rightarrow\text{H+(g)+e-})}$ /kJ mol <sup>-1</sup>	<sup>d</sup> $\Delta G_{\text{hydration}}^{\text{(H•(g)}\rightarrow\text{H•(aq))}}$ /kJ mol <sup>-1</sup>	U <sup>e</sup> /eV	r <sup>o f</sup> /Å
H <sub>3</sub> O <sup>+</sup>	-624.6	1313.8	13.5	-7.0	1.0
H <sub>5</sub> O <sub>2</sub> <sup>+</sup>	-750.9	1313.8	13.5	-5.7	2.2
H <sub>7</sub> O <sub>3</sub> <sup>+</sup>	-819.8	1313.8	13.5	-5.0	3.2
H <sub>9</sub> O <sub>4</sub> <sup>+</sup>	-867.7	1313.8	13.5	-4.5	3.6
H <sub>11</sub> O <sub>5</sub> <sup>+</sup>	-901.9	1313.8	13.5	-4.1	5.0
H <sub>15</sub> O <sub>7</sub> <sup>+</sup>	-1060.4	1313.8	13.5	-2.5	5.4
H <sub>21</sub> O <sub>10</sub> <sup>+</sup>	-993.7	1313.8	13.5	-3.2	5.9
H <sub>27</sub> O <sub>13</sub> <sup>+</sup>	-1049.0	1313.8	13.5	-2.6	6.4

<sup>a</sup>Estimated through Scheme S1 at 298 K.

<sup>b</sup>Hydration free energies are arithmetically averaged from the three models computed in reference S9. See also references S10 and S11 for detailed discussions of existing data.

<sup>c</sup>Taken from reference S2.

<sup>d</sup>Data calculated in reference S12 for T = 300 K, assuming H<sub>2</sub> and H• have identical solvation energies.

<sup>e</sup>Estimated absolute potential.

<sup>f</sup>Estimated spherical, hydrated proton radius (using bond length estimates given in reference S9).

## References

- S1 See, for example, R. Parsons, in A. J. Bard, R. Parsons, J. Jordan (eds.), *Standard Potentials in Aqueous Solution*, IUPAC, Marcel Dekker, Inc., New York, 1985, p.13.
- S2 S. Trasatti, *Pure Appl. Chem.*, 1986, **58**, 955.
- S3 J. Bonin, C. Costentin, C. Louault, M. Robert, J.-M. Savéant, *J. Am. Chem. Soc.*, 2011, **133**, 6668.
- S4 J. E. Halls, N. S. Lawrence, J. D. Wadhawan, *J. Phys. Chem. B*, 2011, **115**, 6509.
- S5 E. Roduner, D. M. Bartels, *Ber. Bunsenges. Phys. Chem.*, 1992, **96**, 1037.
- S6 W. Zhuang, X. Chen, J. Cai, G. Zhang, H. Qiu, *Colloids Surf. A*, 2008, **318**, 175.
- S7 Y. Montet, P. Amara, A. Volbeda, X. Vernede, E. C. Hatchikian, M. J. Field, M. Frey, J. C. Fontecilla-Camps, *Nature Struct. Biol.*, 1997, **4**, 523.
- S8 See, for example, K. A. Vincent, A. Parkin, F. A. Armstrong, *Chem. Rev.*, 2007, **107**, 4366.
- S9 J. A. Mejías, S. Lago, *J. Chem. Phys.*, 2000, **113**, 7306.
- S10 M. D. Tissandier, K. A. Cowen, W. Y. Feng, E. Gundlach, M. H. Cohen, A. D. Earhart, J. V. Coe, T. R. Tuttle, Jr., *J. Phys. Chem. A*, 1998, **102**, 7787.
- S11 W. A. Donald, R. D. Lieb, J. T. O'Brien, M. F. Bush, E. R. Williams, *J. Am. Chem. Soc.*, 2008, **130**, 3371.
- S12 H. Gai, B. C. Garrett, *J. Phys. Chem.*, 1994, **98**, 9642.